Published in final edited form as:
Magn Reson Med. 2012 September ; 68(3): 741–750. doi:10.1002/mrm.23284.

Retrospective Reconstruction of High Temporal Resolution Cine Images from Real-Time MRI using Iterative Motion Correction

Michael S. Hansen[1], **Thomas S. Sørensen**[2], **Andrew E. Arai**[1], and **Peter Kellman**[1]

[1]National Heart, Lung, and Blood Institute, National Institutes of Health, Bethesda, MD, USA

[2]Department of Computer Science and Institute of Clinical Medicine, Aarhus University, Aarhus, Denmark

Abstract

Cardiac function has traditionally been evaluated using breath-hold cine acquisitions. However, there is a great need for free breathing techniques in patients who have difficulty holding their breath. Real-time cardiac MRI is a valuable alternative to the traditional breath-hold imaging approach but the real-time images are often inferior in spatial and temporal resolution. This paper presents a general method for reconstruction of high spatial and temporal resolution cine images from a real-time acquisition acquired over multiple cardiac cycles. The method combines parallel imaging and motion correction based on non-rigid registration and can be applied to arbitrary *k*-space trajectories. The method is demonstrated with real-time Cartesian imaging and Golden Angle radial acquisitions and the motion corrected acquisitions are compared to raw real-time images and breath-hold cine acquisitions in ten (N=10) subjects. Acceptable image quality was obtained in all motion corrected reconstructions and the resulting mean image quality score was a) Cartesian real-time: 2.48, b) Golden Angle real-time: 1.90 (1.00–2.50), c) Cartesian motion correction: 3.92, d) Radial motion correction 4.58, e) Breath-hold cine: 5.00. The proposed method provides a flexible way to obtain high quality, high-resolution cine images in patients with difficulty holding their breath.

Introduction

Cardiac MRI is an accepted reference standard for evaluating cardiac function. The preferred imaging strategy is a breath-hold steady state free precession acquisition with retrospective ECG gating for full coverage of the cardiac cycle (1,2). Although this technique produces reliable results in most patients, it remains a challenge to obtain good quality images in a significant number of patients who have arrhythmias or difficulty with breath holding. In such patients, real-time MRI is a valuable alternative (3–6). The image quality obtained with real-time MRI sequences is, however, not on par with a successful ECG gated, breath-hold acquisition; typically, the spatial and temporal resolution is compromised and SNR is reduced (7). It would be of great clinical benefit if there was a way to obtain the image quality of a breath-hold cine acquisition with free breathing real-time MRI techniques.

Real-time MRI can be acquired over multiple cardiac cycles during free breathing and there is potential for improving the image quality of real-time acquisitions, retrospectively, by

Corresponding Author: Michael S. Hansen, National Institutes of Health, Building 10, B1D405, 9000 Rockville Pike, Bethesda, MD 20814, USA, Phone: +1-301-496-1457, Cell: +1-301-412-9671, michael.hansen@nih.gov.

Disclosures:
NIH and Siemens Medical Systems have a Cooperative Research and Development Agreement (CRADA).

combining data covering multiple cardiac cycles. For Cartesian acquisitions, it has been shown that real-time images from multiple cardiac cycles can be averaged to improve the SNR (8). In that work, the individual real-time images from a given point in the cardiac cycle were registered using non-rigid registration and after discarding the frames with the largest respiratory motion excursion, the remaining images were averaged for improved SNR. The underlying spatial or temporal resolution of the real-time images was not improved using this technique but a second technique was developed where the temporal resolution was enhanced(9). In the proposed approach, the real-time images from matching time points in the cardiac cycle were again registered and warped to match each other, but instead of performing a simple averaging, the image data were transformed back into *k*-space and new datasets were reassembled based on the actual acquisition time of the individual *k*-space lines such that the effective temporal resolution of the resulting images was improved. The key insight of this paper was that because the respiratory motion is relatively low frequency compared to the cardiac contraction, it is possible to determine the deformation due to respiration from the relatively low temporal resolution real-time acquisitions and then subsequently incorporate this knowledge into a reconstruction with substantially higher temporal resolution. Although this technique was shown to be robust, it did have some limitations. Firstly, it only worked with Cartesian datasets or trajectories where it is possible re-sample acquired *k*-space profiles without contamination from profiles acquired at other time points. Secondly, a high acceleration factor (rate 4) was used for the underlying real-time images. The high acceleration factors can cause a substantial up-front reduction in SNR in the real-time images and this reduction in SNR can propagate into the final images. Thirdly, parallel imaging was not employed in the final reconstruction of the reassembled *k*-space datasets and therefore it was necessary to image for a relatively long time (60 seconds per slice) to ensure that enough data would be available after respiratory motion compensation of each cardiac phase. Standard SENSE reconstruction cannot be applied even in the Cartesian sampling case, since the binning of data may cause an irregular under sampling pattern *k*-space. The current paper demonstrates that these limitations can be overcome when a more general formulation of the motion correction reconstruction problem is used.

In 2005, Batchelor, et al. (10)presented a matrix description of general motion correction for multi-shot imaging. In their framework, the description of deformation is integrated into the encoding equations and inverted as part of the reconstruction problem. Briefly, encoding is described as a matrix multiplication in which the encoding matrix is a composite matrix consisting of a) deformation, b) sensitivity encoding using multiple receiver coils, c) Fourier transform to *k*-space, and d) sampling on an arbitrary trajectory. The reconstruction problem consists of inverting this composite matrix; this can for instance be achieved using the conjugate gradient method. The method described by Batchelor, et al. relies on having a description of the deformation (deformation maps) of the imaged object at the time when the individual lines in *k*-space were acquired. However, it does not give very specific ideas as to how such deformation maps can be obtained in the general case.

In this paper, we aim to use the principle of reconstruction using different temporal resolutions to obtain accurate deformation maps that can be integrated into a general reconstruction equation and allow for motion compensated reconstruction of free breathing cardiac datasets acquired with arbitrary *k*-space trajectories. We demonstrate that the technique can be used with Cartesian real-time acquisitions and additionally we propose to use the Golden Angle radial acquisition scheme (11)to acquire the real-time data. The specific advantage of this Golden Angle real-time acquisition strategy is that it is possible reconstruct images with arbitrary temporal resolution at arbitrary points in time.

Materials and Methods

Reconstruction Strategy

The proposed reconstruction strategy is based on being able to reconstruct the acquired data real-time imaging data with different temporal resolutions. Specifically the data are reconstructed with three different temporal resolutions as outlined in Fig. 1, which describes the steps involved in reconstructing an image for a single cardiac phase. Initially a time average of all the acquired data is generated. This served as basis for calculation of coil sensitivity maps and a regularization mask used in later reconstruction steps. Subsequently, real-time images centered on the desired time point in the cardiac cycle (one image for each RR interval) are reconstructed with a modest temporal resolution (*wide window data*). These real-time images do not necessarily have the temporal resolution that would be needed to accurately quantify cardiac function in terms of stroke volume etc., but the temporal resolution is sufficient to determine the deformation and translation of the heart due to respiration. After a respiratory gating procedure (described below) the remaining real-time (within an acceptance window) images are registered using a non-rigid registration algorithm to a reference respiratory phase and deformation maps corresponding to each cardiac cycle are obtained. Based on the desired temporal resolution, a limited number of *k*-space profiles (*narrow window data)* are selected from each cardiac cycle surrounding the target time in the cardiac cycle. This set of gated narrow window data with associated deformation maps is fed into a conjugate gradient reconstruction (described in more detail below), which incorporates coil information (parallel imaging) and motion correction in an integrated fashion.

The procedure for obtaining the low temporal resolution (wide window) real-time images depends on the employed *k*-space trajectory. In this study, we explored two different *k*-space trajectories: Cartesian and Golden Angle radial (11) as detailed below. Briefly, the Cartesian data were acquired using rate 4 TSENSE (12)and the images that were used in the image registration procedure were obtained by interpolating frames corresponding to the center of each narrow window selection. The Golden Angle radial acquisition enables reconstruction of frames with arbitrarily wide temporal windows centered at the same time point as the narrow window selections. The wide temporal window Golden Angle radial images were reconstructed using an iterative non-Cartesian SENSE reconstruction (13).

Motion Correction Reconstruction

The reconstructed image for each cardiac phase is obtained using an iterative conjugate gradient reconstruction scheme (Figure 2) inspired by the framework outlined by Batchelor et al. (10). The encoding equation describing the imaging experiment can be written as:

$$\mathbf{m}=\mathbf{E}\rho, \quad [1]$$

where **m** is a vector containing all measured data, **ρ** is a vector containing all complex signal values of the object and **E** is the encoding matrix describing the encoding from image space to *k*-space. **E** contains all encoding terms including a) deformation, b) coil sensitivities, c) Fourier transform to *k*-space, and d) sampling on *k*-space trajectory. Specifically,

$$\mathbf{e}_i=\Xi_i\mathbf{FSD}_i \quad [2]$$

where $\mathbf{e}_i$ designates a row in matrix **E** describing the encoding of one *k*-space location for a single receive coil. $\mathbf{D}_i$ is a matrix, which defines the deformation of the object at the time when *k*-space location *i* was sampled. In practice this matrix can be expressed as a sparse matrix, which contains the interpolation coefficients needed to resample the object after

deformation. The size of matrix $\mathbf{D}_i$ is $N_p \times N_p$ where N_p is the number of pixels in the image. Each row of the matrix contains mostly zeros except for the columns corresponding to pixels that would contribute to a given pixel in the warped image representation of the object. The number of non-zero entries in each row of the deformation matrix is determined by the interpolation kernel. In this study, bi-linear interpolation was used and consequently, $\mathbf{D}_i$ has only 4 non-zero entries per row in the implementation used here. **S** is a diagonal matrix with the complex coil sensitivity values for a specific coil element along the diagonal. **F** is the Fourier transform from image space to *k*-space and Ξ_i represents the operation of sampling point *i* in *k*-space, i.e. sampling a particular location on the Cartesian grid in Cartesian imaging or interpolating a certain sample in a non-Cartesian acquisition. The coil sensitivities are obtained from a time average of all the acquired data using the procedure described by Walsh et al. (14)

The solution to Eq. [1] is found by solving:

$$(\mathbf{E}^H\mathbf{E}+\lambda^2\mathbf{L}^H\mathbf{L})\boldsymbol{\rho}=\mathbf{E}^H\mathbf{m} \quad [3]$$

where **L** is a diagonal regularization matrix where each of the diagonal elements correspond to the reciprocal of the estimated signal intensity as obtained from a time average of the image and λ is a regularization parameter used to adjust the trade-off between data consistency and regularization. In practice, a conjugate gradient solver (15)was used to obtain the solution. During each conjugate gradient iteration, it is necessary to multiply a search vector with the system matrix ($\mathbf{E}^H\mathbf{E} + \lambda^2 \mathbf{L}^H\mathbf{L}$). It is possible to perform this operation without explicitly forming the system matrix or the encoding matrix **E**. Let **A** denote the system matrix ($\mathbf{E}^H\mathbf{E} + \lambda^2 \mathbf{L}^H\mathbf{L}$), then multiplication $\mathbf{Ax} = \mathbf{b}$ can be performed in a memory and computationally efficient manner as outlined in Algorithm 1. For every motion state (RR interval with different deformation due to respiration) from which data were included, the search vector is warped according to the corresponding deformation map. This operation is a resampling of the vector **x** as described by the interpolation coefficients in $\mathbf{D}_m$. Then for each coil, the resulting warped search vector is sampled at the appropriate *k*-space locations and the resulting *k*-space data are inserted back into an empty *k*-space (this could include a gridding operation in the case of non-Cartesian sampling), inverse Fourier transformed to image space, multiplied with the conjugate of the coil sensitivities, and added up for all coils. Finally the transpose of the warping operation is applied. It is important to note that the multiplication with $\mathbf{D}_m^H$ is not equivalent to the inverse of the deformation, which may not be well defined. As mentioned the warping matrix **D** can be stored as a sparse matrix and applying the transpose is simply multiplying with the transpose of this sparse matrix. In practice, the sparse representation of **D** was stored in a form convenient for applying $\mathbf{D}_m^H$, whereas the forward operation $\mathbf{D}_m$ was implemented as a pixel-wise warping based on the deformation field obtained during registration. For non-Cartesian sampling trajectories the gridding was performed as per Jackson, et al. (16) with a Kaiser-Bessel gridding kernel of width 4 (β =18.5547) and an oversampling factor of 2.

Non-rigid Registration

The deformation maps needed to form the $\mathbf{D}_m$ matrices in Algorithm 1 were obtained using a non-rigid optical flow registration algorithm as per Horn and Schunck (17)as described in reference (18). A multi-resolution approach was used to increase the “capture range” of deformations between the source and reference images. Starting at the lowest resolution every source image was registered to the corresponding reference image resulting in a deformation vector field. At increasing resolutions the source images were resampled from the vector field obtained at the previous resolution level and registered to the corresponding

reference image. An iterative Jacobi solver was used to solve the resulting linear system at each resolution.

Imaging Parameters

Data were acquired using Siemens Espree and Avanto scanners (Siemens Medical Solutions, Erlangen, Germany) and a 32 channel cardiac receive array (Invivo, Gainesville, FL). A Steady State Free Precession (SSFP) sequence was used with 50-degree flip angle. Echo time and repetition time was kept at 1.54 ms and 3.07 ms respectively for all measurements. Matrix base resolution was 256 and bandwidth was set at ~1000 Hz/pixel (sampling dwell time of 2 μs with two-fold readout oversampling) and slice thickness was 6mm.

For Cartesian imaging, field of view (FOV) was set at 360–380 mm with a rectangular field of view percent of 75–100 to accommodate subject size. Care was taking to make sure that the subject was sufficiently covered by the FOV since several components of the reconstruction rely on SENSE reconstruction principles that become less reliable when fold-over artifacts are present. The number of acquired phase encoding lines was 144–186 resulting spatial resolutions of 1.4–1.5x1.9–2.0 mm^2. A breath-hold segmented acquisition was acquired with retrospective ECG gating and 2-fold parallel imaging acceleration (GRAPPA with 24 reference lines). The cardiac cycle was covered with 30 reconstructed phases in a 6–8 second acquisition depending on heart rate. The resulting temporal resolution was ~30 ms per frame. Additionally a real-time acquisition was acquired using the same matrix size and FOV but with 4-fold parallel imaging acceleration and a resulting temporal resolution of 110–142 ms. Approximately 30 seconds of real-time data were acquired.

Radial acquisitions were acquired with a square matrix of 256x256 and FOV of 360-380×360-380 mm^2 resulting in a spatial resolution of 1.4-1.5×1.4-1.5 mm^2. Real-time radial datasets (30 second acquisition) were acquired using the Golden Angle profile ordering scheme (11). With this scheme each acquired profile is rotated by $\pi/((\sqrt{5}+1)/2)$ = 1.94 radians or 111.25 degrees. As a result of this profile rotation, each new profile will divide the biggest gap between any two profiles according to the golden ratio. Because of this property it is possible to select a number of profiles from the acquisition using an arbitrarily placed temporal window of arbitrary width and the resulting *k*-space coverage will be close to uniform.

ECG Timing and Respiratory Motion Gating

All *k*-space profiles were acquired with ECG time stamps (time since last trigger). For each ECG time stamp, the cardiac cycle length was determined as the ECG time stamp of the last *k*-space profile before a new trigger was detected and the average cardiac length was calculated. The relative timing of each *k*-space profile was calculated with respect to a normalized cardiac cycle length (the average RR interval). In general, the normalization of the cardiac cycles can be linear or one of several non-linear schemes (19)taking into account that diastolic duration changes more than systolic duration as heart rate changes. In this study a non-linear scheme was used.

Thirty cardiac phases were reconstructed from each of the real-time acquisitions (Cartesian and Golden Angle radial). For a given cardiac phase, the relative time in the cardiac cycle was determined and data for this particular cardiac phase was selected as follows. Based on the relative cardiac cycle timing of each *k*-space profile a certain number of profiles (*narrow window*) were selected from each of the covered cardiac cycles. In all reconstructions presented here, a narrow window of 10 *k*-space profiles (~30 ms) was used.

To determine the respiratory deformation field associated with each of the covered cardiac cycles, a low temporal resolution image for each covered cardiac cycle was needed (referred to as *motion state images*). In the case of Cartesian real-time imaging, the motion state images were found by linear interpolation of the two real-time images immediately before and after the central *k*-space profile in the narrow window. In the Golden Angle acquisition it was possible to place a wide reconstruction window centered on the central profile of the narrow window and perform a non-Cartesian SENSE reconstruction on this selection to obtain the motion state images. In the results presented here a wide window of 100 *k*-space profiles was used (temporal resolution of ~300ms)for radial imaging.

In order to determine which motion state images should serve as the registration target when determining the deformation fields, the following procedure inspired by Ledesma-Carbayo, et al.(20)was used to find the RR interval with the most prevalent respiratory position. First the root-mean-square (RMS) difference of each of the motion state images with all other motion state images was calculated. These differences were accumulated in an $N_{ms} \times N_{ms}$ matrix where N_{ms} is the total number of motion states for a given reconstruction. Subsequently, each row was sorted (low to high) and for every row and the median RMS difference was determined. The motion state associated with the lowest median RMS difference was chosen as the registration target. At this stage respiratory gating was employed. In the results presented here the data from the motion states with the 50% lowest RMS differences was kept and the rest was discarded. To ensure that all cardiac phases in a reconstruction were using the same cardiac cycle as reference, this procedure was only applied during the reconstruction of the first cardiac phase and when reconstruction subsequent cardiac phases, the motion state image that was the closest in time to the registration target of the first cardiac phase was used.

Experimental Measurements

Ten (N=10) patients and volunteers were studied with a) Cartesian breath-hold cine, b) Real-time Cartesian free breathing, and c) Real-time Golden Angle radial imaging. The local Institutional Review Board approved the study protocol and all subjects gave written informed consent. A single mid ventricular short-axis slice was acquired in the same orientation with all the acquisitions. In some subjects an additional long axis acquisition was performed. Low temporal resolution real-time images were reconstructed with the *wide window* temporal resolutions described above and motion corrected reconstructions were obtained with the proposed algorithm. In order to determine the effect of motion correction, the proposed algorithm was used with the motion fields as determined by the non-rigid registration and with the motion field set to zero (assuming no respiratory motion).

The reconstructed images were converted to AVI movie files, viewed in random order, and assigned a quality score between 1 and 5 (increment of 0.5), with 1 being the worst score and 5 being the best. A score of 5 (excellent) was given to a reconstruction without noteworthy artifacts, high contrast between blood and myocardium, and sharp borders and distinct appearance of fine structural details. A score of 4 (good) was given to a reconstruction with some insignificant artifacts but with adequate image quality to determine cardiac function. A score of 3 (fair) was given to images with borderline image quality, which could be used to evaluate global cardiac function and regional function. A score of 2 (poor) was given to images with inadequate image quality for determining regional function, and a score of 1 (non diagnostic) was given when images were inadequate for evaluating global cardiac function. Two reviewers scored each image and the average score of the two reviewers was used as the combined score. In addition to assigning scores to the cine breath-hold acquisitions and the motion corrected reconstructions, the raw real-time images (used in the non-rigid registration) were also scored for comparison. The scores from the different

reconstruction types were compared using a one-way ANOVA with Tukey Honestly Significant Difference(HSD)post-hoc testing using R (R for Mac OS X v1.40).

Results

Figure 3 is an example of how then on-rigid registration minimizes respiratory motion. Example frames are shown from one subject in diastole and systole and *y-t* (spatial-temporal)plots are used to visualize the respiratory excursion in this particular subject. The non-rigid registration aligns the different respiratory states quite effectively.

Figure 4 shows example reconstruction results using both Cartesian and Golden Angle Radial acquisition schemes in the same volunteer. Reconstructions are shown using respiratory gating but no motion correction (simple averaging), using the motion correction algorithm with motion maps set to zero (parallel imaging only), and finally the motion corrected reconstruction result. The motion correction algorithm is able to remove the blurring of the ventricle wall, which occurs when data from multiple cardiac cycles are averaged. In general the subjects included in this study showed a range of respiratory motion and in some cases most of the gain in image quality came from respiratory gating alone and in others the motion correction provided by the non-rigid registration provided substantial improvement of cardiac wall sharpness. A three-chamber view from one subject is shown in Fig. 5.

The quantitative results of the motion quality scoring are summarized in Fig. 6. The mean (range) scores from the different reconstructions were: a) Cartesian real-time: 2.48 (1.75–3), b) Golden Angle real-time: 1.90 (1.00–2.50), c) Cartesian Motion Correction: 3.92 (3.25–4.5), d) Radial Motion Correction 4.58 (4.00–5.00), e) Breath-Hold Cine: 5 (5.00-5.00). There was a significant difference ($p < 0.01$) between the breath-hold cine acquisitions and all other reconstruction types with the breath-hold cine acquisitions scoring higher in all cases. The motion corrected reconstruction had significantly ($p < 0.01$) better scores than the raw real-time images and there was also a significant difference ($p < 0.01$) between Cartesian and Radial motion corrected acquisitions. Example motion corrected images with the best and worst scores are shown in Fig. 7. There are some clearly visible streaking artifacts in the worst scoring images (particularly in the Cartesian motion corrected reconstructions). These streaking artifacts extend from the liver into the heart in some cases and when viewed as a movie they contribute to some flickering artifacts in the liver and heart. Those artifacts did not render the images non-diagnostic from a cardiac function point of view, but they contributed to the lower scores.

Discussion

This paper presents a generic method for reconstruction of high spatial and temporal resolution images from real-time cardiac acquisitions. The method is a generalization of a previously published principle (9). The previously published method relied on Cartesian sampling and on having a fully sampled *k*-space at the end of the motion correction procedure to avoid aliasing artifacts in the reconstructed images. With the method presented in this paper it is possible to accommodate arbitrary *k*-space sampling strategies, and since parallel imaging is integrated into the final reconstruction step, it is not necessary to have a fully sampled dataset. This is accomplished by using a reconstruction principle proposed by Batchelor, et al.(10)in which the deformation caused by respiratory motion and the sensitivity encoding is integrated into one reconstruction problem. The method can be used to reconstruct Cartesian real-time acquisitions and this paper also proposes the Golden Angle Radial acquisition strategy as a flexible way of acquiring the required real-time data.

The Golden Angle trajectory is attractive for this application because it allows reconstruction with arbitrary temporal resolution at arbitrary points in time.

The quality comparison showed that all motion corrected reconstructions had sufficient quality for determining cardiac function. Not surprisingly, the image quality of the motion corrected reconstructions was better than the raw real-time images. The temporal resolution of the real-time images was much lower (~125 ms for Cartesian, ~300ms for Radial) than the motion corrected reconstructions (~30 ms) and consequently, the myocardial motion was not appropriately captured in systole resulting in blurring of the myocardial tissue. It should be noted that the real-time imaging sequences used in this study had high spatial resolution (and consequently lower temporal resolution) and a sequence optimized for capturing cardiac motion in real-time would probably have been set up with a different tradeoff between spatial and temporal resolution. This explains why the differences in image quality scores are relatively large in this particular study. When comparing the motion corrected real-time acquisitions and the traditional breath-hold, segmented cine acquisitions, the breath-hold cine acquisitions were found to have higher quality scores. In this study all patients were capable of holding their breath for the duration of the acquisition and consequently it is expected that the breath-hold acquisitions have the highest possible scores. A more thorough comparison would include patients with difficulty holding their breath. The radial real-time acquisitions had a higher quality score than the Cartesian real-time motion corrected acquisitions. The Cartesian motion correction procedure as described in this paper relies on a rate 4 parallel imaging reconstruction to determine the motion fields. The high acceleration factor can lead to some noise in the deformation maps, which may propagate into the final reconstructions. The Golden Angle radial acquisitions on the other hand included considerably more data (100 projections per image), which may have resulted in better real-time images for the motion registration. Furthermore, residual motion in the real-time images generally manifests itself as blurring and non-coherent aliasing in the radial acquisitions whereas some fast breathing can cause distinct aliasing of the chest wall in the Cartesian real-time images. This again provides the Cartesian approach with a less optimal starting point for the motion registration. Finally, there is a tendency for residual artifacts to look more benign (diffuse) in the radial acquisitions, which may also have contributed to the difference in quality scores.

The primary purpose of this paper was to introduce a new reconstruction algorithm and because of the limited scope there are some limitations: a) the presented method does not include arrhythmia rejection, which would be required for scanning patients with irregular heart rhythm, b) only a small number of subjects were studied. Specifically, all subjects were able to hold their breath and consequently the breath-hold acquisitions came out better on average than they would in a typical clinical population, c)the studies focused mainly on the short axis orientation, which is most commonly used for cardiac function assessment, and although other orientations were explored, they were not studied systematically, d) the reconstruction software has not been optimized and the reconstruction time is on the order of ~15 minutes for the Cartesian acquisitions and ~ 2 hours for the golden angle radial acquisitions, e) the reconstruction algorithm has a number of tunable parameters (respiratory gating factor, regularization factors, choice of registration algorithm, etc.) and the appropriate setting of these parameters was not explored in a systematic way, the settings used here were found to work well in the cases studied in this paper, and finally f) this study does not investigate the effect of the motion correction on the parallel imaging performance (*g*-factor). The motion deformation introduces additional terms in the encoding matrix, which may affect the conditioning, but since the coils sensitivities vary slowly in space and the respiratory motion is relatively modest (due to the respiratory gating) no great effect on parallel imaging performance is expected.

There are some modifications to the algorithm that may improve the robustness of the algorithm for a wider range of applications. The proposed implementation of the method relies on accurate coil sensitivity maps, which are obtained by averaging the entire dataset. Such coil sensitivity maps can be corrupted in which case it might be beneficial to calculate time varying coil sensitivity maps using a sliding window. In this study it was not found to be necessary to add this feature, but it is fully supported by the algorithm and can be implemented in a straightforward fashion by making **S** in Algorithm 1 be dependent on motion state, Furthermore, the motion deformation (multiplication with $\mathbf{D}_m$ and $\mathbf{D}_m^{\mathrm{H}}$ in Algorithm 1) was based on bi-linear interpolation. This will lead to some broadening of the image point spread function, which can be mitigated with a better interpolation kernel, e.g. bicubic interpolation. The matrix **D** can still be expressed as a sparse matrix, but it will have more non-zeros entries and the computational complexity of the algorithm will increase. In the present study we did not find a need for this added complexity, but a more thorough analysis for a given application may be needed to determine the appropriate interpolation kernel.

Future work will be aimed at selecting appropriate reconstruction parameters for a broad patient population and implementing an optimized version of the reconstruction using GPU technology (21–23)such that the technique can be appropriately integrated into a clinical workflow. This would enable proper testing of the technique in a wide group of patients.

Conclusion

We have presented a general method for obtaining high spatial and temporal resolution cine images from free-breathing real-time cardiac MRI. The technique can be applied to arbitrary *k*-space trajectories and compared to previously published approaches it relaxes the sampling constraints since parallel imaging is integrated into the final reconstruction step.

Acknowledgments

This work is supported by the Division of Intramural Research, National Heart Lung and Blood Institute, National Institutes of Health, USA.

References

1. Lenz GW, Haacke EM, White RD. Retrospective cardiac gating: a review of technical aspects and future directions. Magn Reson Imaging. 1989 Oct; 7(5):445–55. [PubMed: 2607896]
2. Carr JC, Simonetti O, Bundy J, Li D, Pereles S, Finn JP. Cine MR angiography of the heart with segmented true fast imaging with steady-state precession. Radiology. 2001 Jun; 219(3):828–34. [PubMed: 11376278]
3. Setser RM, Fischer SE, Lorenz CH. Quantification of left ventricular function with magnetic resonance images acquired in real time. J Magn Reson Imaging. 2000 Sep; 12(3):430–8. [PubMed: 10992310]
4. Plein S, Smith WHT, Ridgway JP, Kassner A, Beacock DJ, Bloomer TN, Sivananthan MU. Qualitative and quantitative analysis of regional left ventricular wall dynamics using real-time magnetic resonance imaging: Comparison with conventional breath-hold gradient echo acquisition in volunteers and patients. J Magn Reson Imaging. 2001 Jul; 14(1):23–30. [PubMed: 11436210]
5. Kaji S, Yang PC, Kerr AB, Tang WH, Meyer CH, Macovski A, Pauly JM, Nishimura DG, Hu BS. Rapid evaluation of left ventricular volume and mass without breath-holding using real-time interactive cardiac magnetic resonance imaging system. J Am Coll Cardiol. 2001 Aug; 38(2):527–33. [PubMed: 11499748]
6. Hori Y, Yamada N, Higashi M, Hirai N, Nakatani S. Rapid evaluation of right and left ventricular function and mass using real-time true-FISP cine MR imaging without breath-hold: comparison

with segmented true-FISP cine MR imaging with breath-hold. J Cardiovasc Magn Reson. 2003 Jul; 5(3):439–50. [PubMed: 12882075]

7. Muthurangu V, Lurz P, Critchely JD, Deanfield JE, Taylor AM, Hansen MS. Real-time assessment of right and left ventricular volumes and function in patients with congenital heart disease by using high spatiotemporal resolution radial k-t SENSE. Radiology. 2008 Sep; 248(3):782–91. [PubMed: 18632528]
8. Kellman P, Chefd'hotel C, Lorenz CH, Mancini C, Arai AE, McVeigh ER. Fully automatic, retrospective enhancement of real-time acquired cardiac cine MR images using image-based navigators and respiratory motion-corrected averaging. Magn Reson Med. 2008 Apr; 59(4):771–8. [PubMed: 18302227]
9. Kellman P, Chefd'hotel C, Lorenz CH, Mancini C, Arai AE, McVeigh ER. High spatial and temporal resolution cardiac cine MRI from retrospective reconstruction of data acquired in real time using motion correction and resorting. Magn Reson Med. 2009 Dec; 62(6):1557–64. [PubMed: 19780155]
10. Batchelor PG, Atkinson D, Irarrazaval P, Hill DLG, Hajnal J, Larkman D. Matrix description of general motion correction applied to multishot images. Magn Reson Med. 2005 Nov; 54(5):1273–80. [PubMed: 16155887]
11. Winkelmann S, Schaeffter T, Koehler T, Eggers H, Doessel O. An optimal radial profile order based on the Golden Ratio for time-resolved MRI. IEEE Trans Med Imaging. 2007 Jan; 26(1):68–76. [PubMed: 17243585]
12. Kellman P, Epstein FH, McVeigh ER. Adaptive sensitivity encoding incorporating temporal filtering (TSENSE). Magn Reson Med. 2001 May; 45(5):846–52. [PubMed: 11323811]
13. Pruessmann KP, Weiger M, Börnert P, Boesiger P. Advances in sensitivity encoding with arbitrary k-space trajectories. Magn Reson Med. 2001 Oct; 46(4):638–51. [PubMed: 11590639]
14. Walsh DO, Gmitro AF, Marcellin MW. Adaptive reconstruction of phased array MR imagery. Magn Reson Med. 2000 May; 43(5):682–90. [PubMed: 10800033]
15. Axelsson, O. Iterative solution methods. New York: Cambridge University Press; 1996.
16. Jackson JI, Meyer CH, Nishimura DG, Macovski A. Selection of a convolution function for Fourier inversion using gridding. IEEE Trans Med Imaging. 1991; 10(3):473–8. [PubMed: 18222850]
17. Horn BKP, Schunck BG. Determining optical flow. Artificial Intelligence. 1981 Aug; 17(1–3): 185–203.
18. Østergaard Noe K, De Senneville BD, Elstr∅m UV, Tanderup K, S∅rensen TS. Acceleration and validation of optical flow based deformable registration for image-guided radiotherapy. Acta Oncol. 2008; 47(7):1286–93. [PubMed: 18661435]
19. Feinstein JA, Epstein FH, Arai AE, Foo TK, Hartley MR, Balaban RS, Wolff SD. Using cardiac phase to order reconstruction (CAPTOR): a method to improve diastolic images. J Magn Reson Imaging. 1997 Oct; 7(5):794–8. [PubMed: 9307903]
20. Ledesma-Carbayo MJ, Kellman P, Hsu L-Y, Arai AE, McVeigh ER. Motion corrected free-breathing delayed-enhancement imaging of myocardial infarction using nonrigid registration. J Magn Reson Imaging. 2007 Jul; 26(1):184–90. [PubMed: 17659545]
21. Hansen MS, Atkinson D, Sorensen TS. Cartesian SENSE and k-t SENSE reconstruction using commodity graphics hardware. Magn Reson Med. 2008 Mar; 59(3):463–8. [PubMed: 18306398]
22. Sorensen TS, Schaeffter T, Noe KO, Hansen MS. Accelerating the nonequispaced fast Fourier transform on commodity graphics hardware. IEEE Trans Med Imaging. 2008 Apr; 27(4):538–47. [PubMed: 18390350]
23. S∅rensen TS, Atkinson D, Schaeffter T, Hansen MS. Real-time reconstruction of sensitivity encoded radial magnetic resonance imaging using a graphics processing unit. IEEE Trans Med Imaging. 2009 Dec; 28(12):1974–85. [PubMed: 19628452]

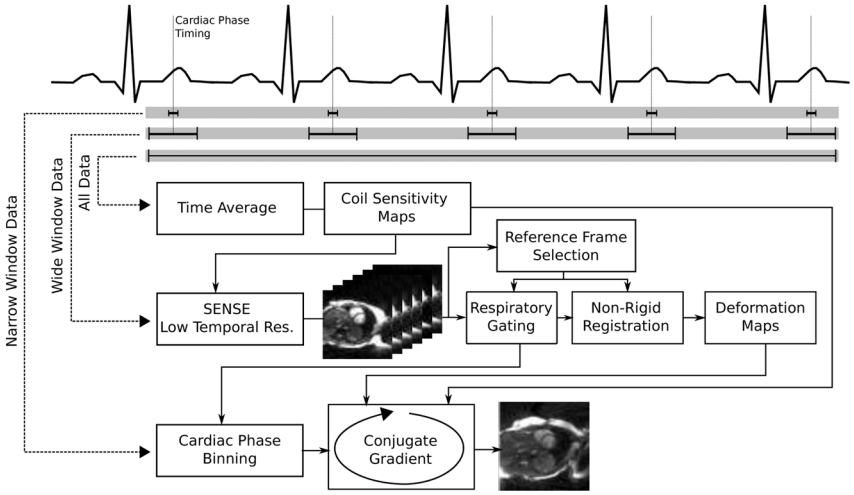

Figure 1.

Reconstruction scheme for a single cardiac phase. Data is processed with 3 different temporal resolutions: 1) a time average of the data is used to obtain coil sensitivity maps, 2) low temporal resolution images (one for each RR interval) are reconstructed using a wide temporal window, and 3) a narrow window selected of data from each RR interval is used in the final reconstruction of each cardiac phase. The wide window images are used to perform respiratory gating and to determine the respiratory deformation associated with each remaining RR interval after the respiratory gating procedure. The narrow window data, coil sensitivity maps, and deformation maps form the input to the conjugate gradient iterative reconstruction (see Fig. 2).

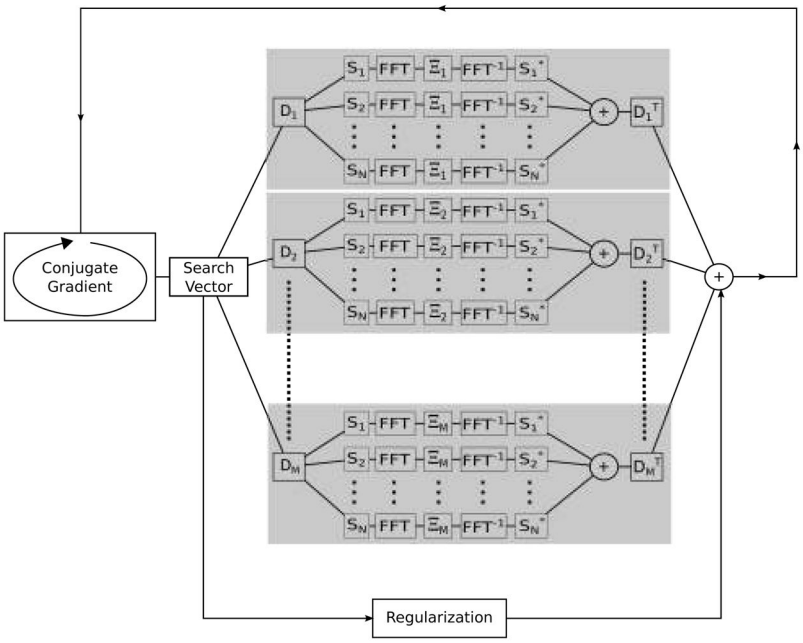

Figure 2.

Iterative reconstruction scheme to solve Eq. [3] using conjugate gradient iterations. In each iteration, a search vector is multiplied with the system matrix (according to Algorithm 1): For every RR interval included (after respiratory gating) in the reconstruction the search vector goes through the following operations (the gray boxes indicate the operations carried out for each RR interval): a) deformation using a deformation map obtained using non-rigid registration ($\mathbf{D}_1$, $\mathbf{D}_2$, …, $\mathbf{D}_M$), b) multiplication with coil sensitivities ($\mathbf{S}_1$, $\mathbf{S}_2$, …, $\mathbf{S}_N$), c) Fourier transform (FFT) to *k*-space and sampling $\mathbf{\Xi}_i$ (possibly on non-Cartesian trajectory), d) Fourier transform back to image space, e) summation over all coils, f) multiplication with the transpose of the deformation matrix. Additionally, the search vector is multiplied with a regularization matrix ($\mathbf{L}^H\mathbf{L}$), which is a diagonal matrix containing the reciprocal expected signal intensity squared as the diagonal elements.

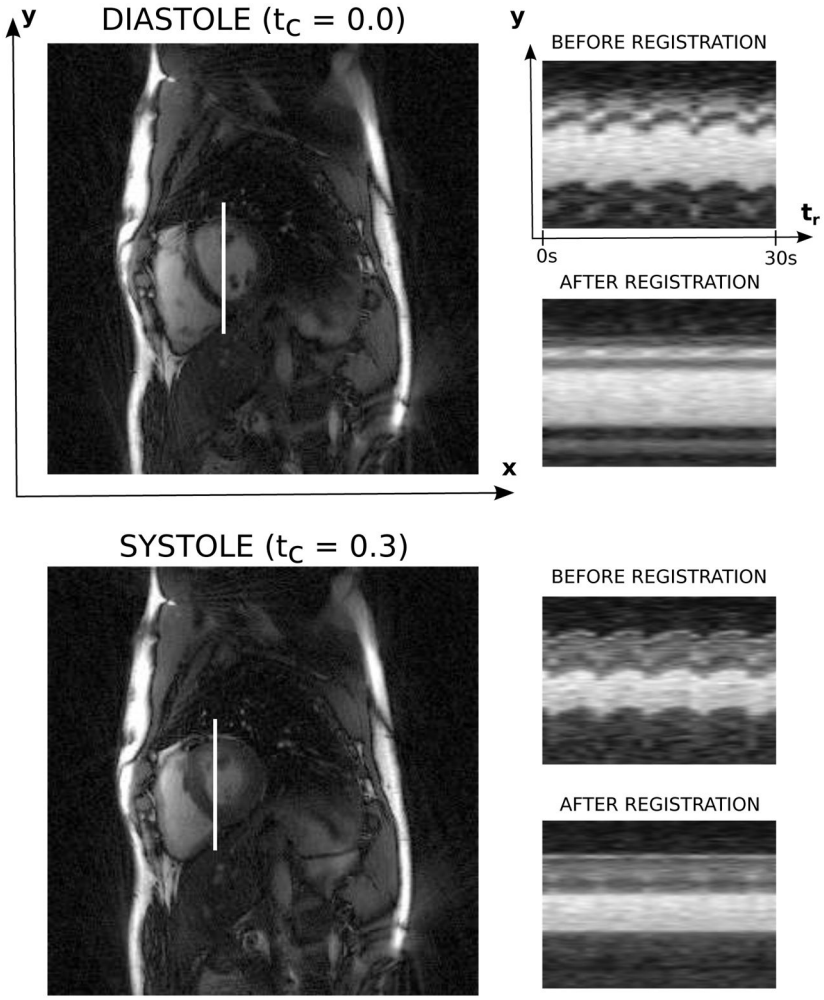

Figure 3.

Series of diastolic and systolic images demonstrate how the non-rigid motion correction minimizes respiratory motion. As outlined in Fig. 1, a series of low temporal resolution images will be generated for each cardiac phase in the target reconstruction. These images will be registered to a reference frame to provide deformation maps. Here is shown examples of the low temporal resolution images from a diastolic phase (relative cardiac phase time t_c = 0.0)and a diastolic phase (t_c = 0.3). On the right is shown *y-t* plots from the position through the heart indicated by the white line. These plots are generated from a single point in the cardiac cycle, one image for each cardiac cycle covered, i.e. they illustrate how the heart moves over the respiratory cycles (respiratory time, t_r). Approximately 5 respiratory cycles are covered in the 30 seconds of imaging.

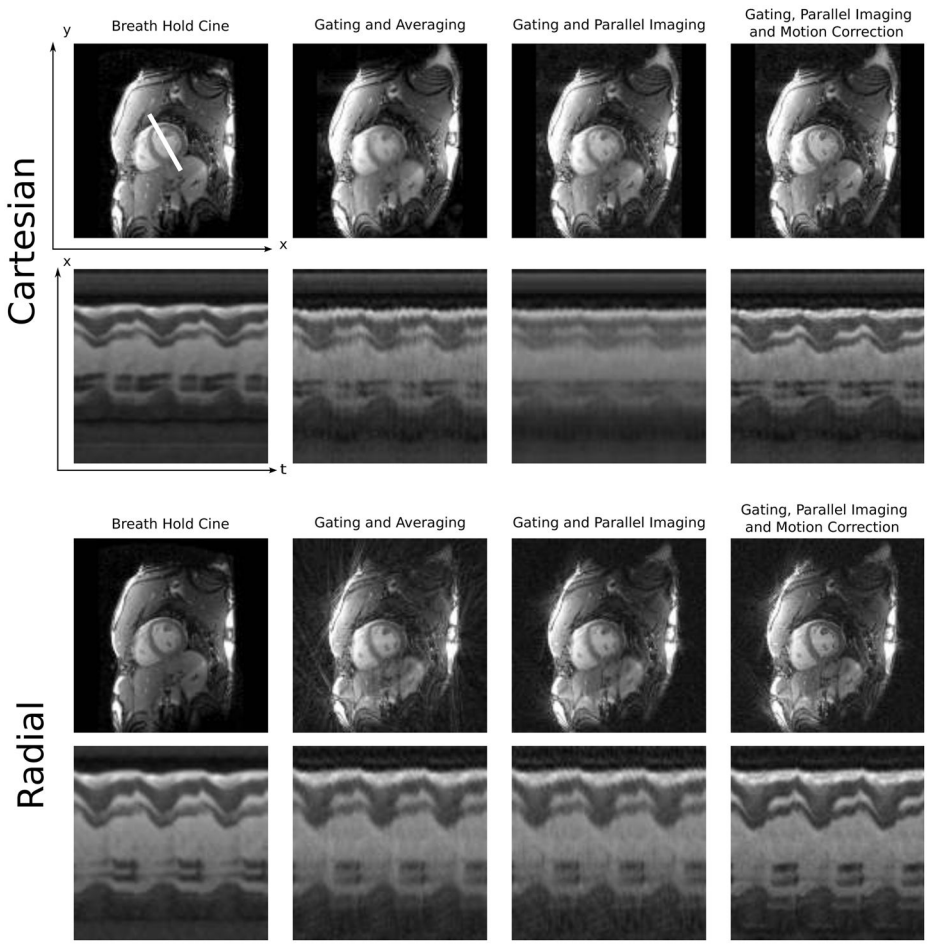

Figure 4.

Comparison of image quality and cardiac motion derived from breath-hold cine and motion corrected free-breathing acquisitions. The top set of images show a Cartesian free-breathing acquisition and the bottom set from the same subject but using a golden angle radial acquisition. The top left (first column) image example in both sets is a Cartesian breath-hold cine reference, which has been repeated to enable easier comparison with the real-time acquisition. For each set of images, the top row is a diastolic frame and the bottom row is an *x-t* (spatial-temporal) plot from the location indicated by the white line. The cardiac cycle has been repeated three times for better illustration of the cardiac dynamics. The second column shows the reconstruction obtained with the gated narrow window data simple inserted into *k*-space and Fourier transformed. Third column shows the effect of actually running this data through the full reconstruction but with the deformation maps set to zero (i.e. assuming no motion) in which case the reconstruction is simply a parallel imaging reconstruction allowing some motion blurring. Finally, the fourth column shows the full motion correction reconstruction providing the closest quality to the breath-hold cine.

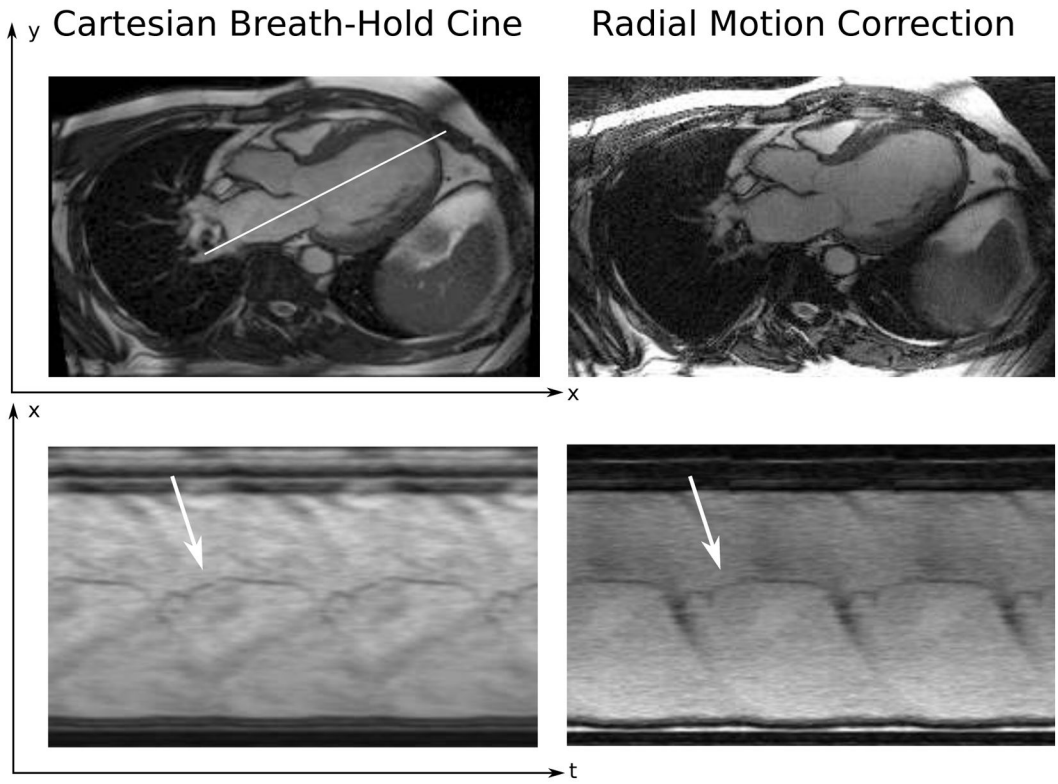

Figure 5.

Three-chamber example from a single subject. The left two panels show a Cartesian breath-hold cine acquisition with an example frame and an *x*-*t* plot from the position marked by the white arrow. The right two panels show approximately the same view from the same subject from a Golden Angle motion corrected acquisition. Notice the delineation of the mitral valve leaflet in the *x*-*t* plots of both acquisitions.

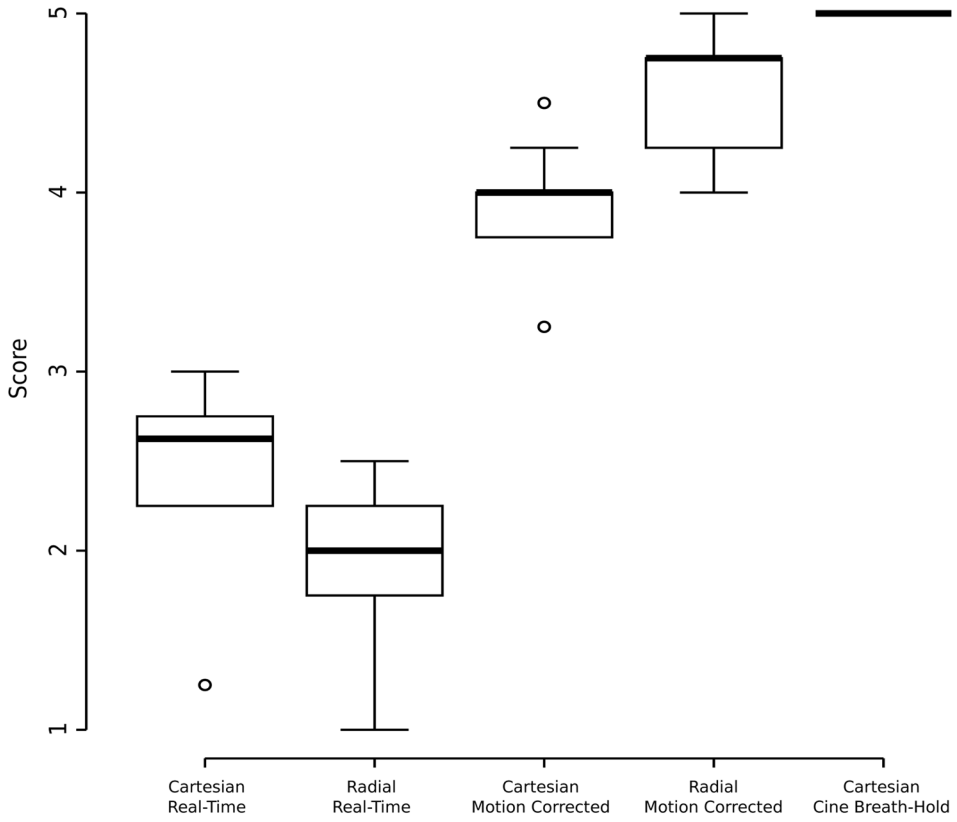

Figure 6.

Box blot of image quality scores from Cartesian real-time, Golden Angle real-time, Cartesian motion correction, Golden Angle Radial motion correction, and breath-hold cine acquisitions. Images were scored by two reviewers and the average of the two reviewer scores were used as the score for a given image series. The mean (range) scores were : a) Cartesian real-time: 2.48 (1.75–3), b) Golden Angle real-time: 1.90 (1.00–2.50), c) Cartesian Motion Correction: 3.92 (3.25–4.5), d) Radial Motion Correction 4.58 (4.00–5.00), e) Breath-Hold Cine: 5 (5.00-5.00). The motion corrected reconstructions had significantly ($p < 0.01$, One way ANOVA with Tukey HSD post hoc testing) higher scores than their real-time counterparts and the breath-hold cine acquisitions were significantly ($p< 0.01$) better than all other reconstruction types.

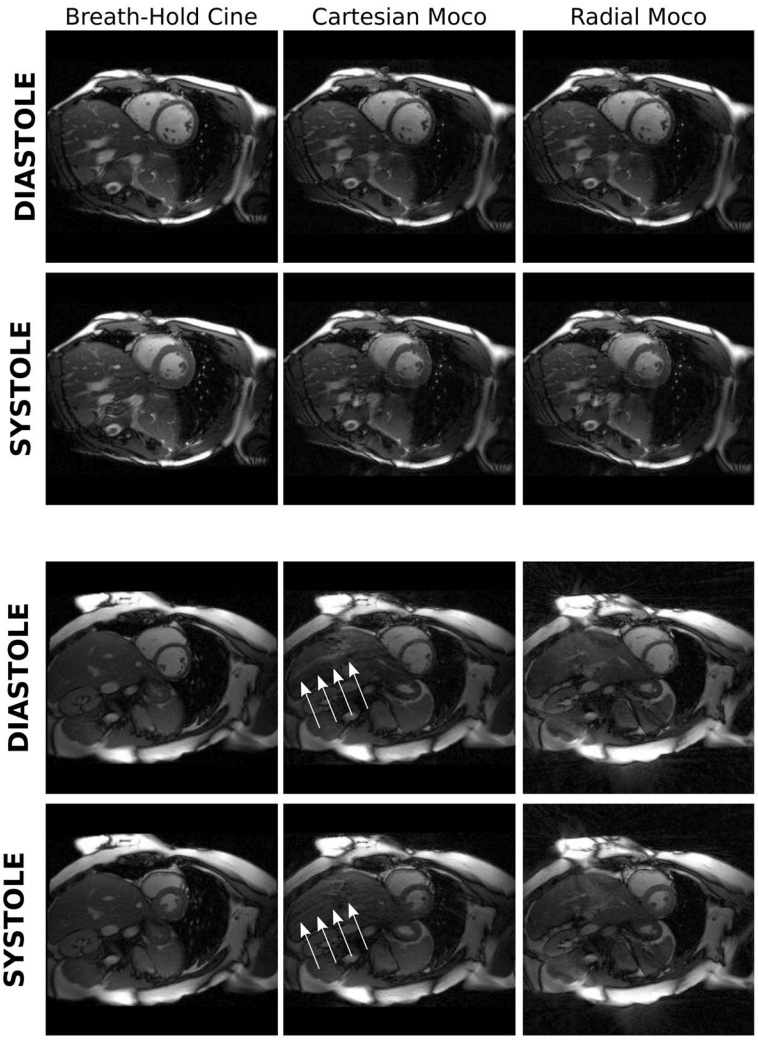

Figure 7.
Example images from the motion correction reconstruction with the best (top), and worst (bottom) scores. The images with the lower quality scores have residual aliasing and motion artifacts (indicated with arrows over the liver). The artifacts stretch into the heart and although they may not interfere with overall cardiac function assessment they do contribute to a lower image quality score for the image series.

Algorithm 1

Multiplication of vector **x** with system matrix ($\mathbf{E}^H\mathbf{E} + \lambda^2\mathbf{L}^H\mathbf{L}$). Result is stored in **b**.

b = 0	(Initialization)
for _ = 1 to number of motion states,	
q = $\mathbf{D}_m\mathbf{x}$	(Warp object)
t = 0	(Initialize motion state)
for *c* = 1 to number of coils,	
w = **Sq**	(Multiply with coil sensitivity)
w = fft(**w**)	(Fourier transform to *k*-space)
z = sample(**w**)	(Sample *k*-space, may include gridding)
k = 0	(empty *k*-space)
insert **z** *into* **k**	(May involve gridding)
k = ifft(**k**)	(Inverse Fourier transform to image)
k = **S*** **k**	(Multiply with conjugate of sensitivities)
t = **t** + **k**	(Sum up coils)
end	
$\mathbf{b}=\mathbf{b}+\mathbf{D}_m^H\mathbf{t}$	(Apply transpose of deformation)
end	
b = **b**+ $\lambda^2\mathbf{L}^H\mathbf{L}\mathbf{x}$	(Add regularization term)